

Parrot Beak-Inspired Metamaterials with Friction and Interlocking Mechanisms 3D/4D Printed in Micro and Macro Scales for Supreme Energy Absorption/Dissipation

Ramin Hamzehei, Mahdi Bodaghi,* Julio Andrés Iglesias Martinez, Qingxiang Ji, Gwenn Ulliac, Muamer Kadic, Changguo Wang, Ali Zolfagharian, and Nan Wu*

Energy absorption and dissipation features of mechanical metamaterials have widespread applications in everyday life, ranging from absorbing shock impacts to mechanical vibrations. This article proposes novel bioinspired friction-based mechanical metamaterials with a zero Poisson's ratio behavior inspired from parrot's beaks and manufactured additively. The mechanical performances of the corresponding metamaterials are studied at both macro and micro scales by experiments and finite element analysis (FEA). An excellent agreement is observed between the FEA and both microscopic and macroscopic scale experiments, showing the accuracy of the developed digital tool. Performances are compared to traditional triangular lattice metamaterials. Both experimental tests and FEA results demonstrate the following advantages: 1) absorbing and dissipating energy per unit of mass (SEA) at large compressive strains without global buckling; 2) bistable deformation patterns including friction-based and interlocking mechanisms; 3) reversible deformation patterns after unloading; 4) shape recovery behavior after a heating-cooling process; and 5) the higher elastic modulus of micro metamaterials compared with their macro counterparts. This is the first demonstration of a bioinspired friction-based design of 3D-printed mechanical metamaterials that feature absorbing/dissipating energy, stability, and reversibility properties to cater to a wide range of sustainable *meta*-cylinders in micro and macro scales.


1. Introduction

Viscoelasticity indicates a property of the materials exhibiting simultaneous viscous and elastic characteristics when undergoing deformation.^[1] When it comes to energy absorption, industrialists frequently consider traditional viscoelastic materials^[1] such as elastomeric rubber for many industrial applications. Viscoelastic materials form a hysteresis loop under applying and releasing mechanical loads. Due to the internal friction of the molecular chains, the area within the loop expresses the dissipated energy in the form of heat. Although practical, most viscoelastic materials exhibit limitations in operational conditions such as excessive heat when the structures, beams, or hinges are particularly heated in volume and face large strains. This could have catastrophic effects on the mechanical characteristics of the structure, leading to an early fatigue failure or even rupture.^[2]

Metamaterials are rationally designed composites aiming at effective material parameters that go beyond those of the ingredient materials.^[3–8] With the advent of three-dimensional (3D) printing technology, the fabrication of complex 3D structures

R. Hamzehei, N. Wu
Department of Mechanical Engineering
University of Manitoba
Winnipeg, Manitoba R3T 5V6, Canada
E-mail: nan.wu@umanitoba.ca

M. Bodaghi
Department of Engineering
School of Science and Technology
Nottingham Trent University
Nottingham NG11 8NS, UK
E-mail: mahdi.bodaghi@ntu.ac.uk

 The ORCID identification number(s) for the author(s) of this article can be found under <https://doi.org/10.1002/adem.202201842>.

© 2023 The Authors. Advanced Engineering Materials published by Wiley-VCH GmbH. This is an open access article under the terms of the Creative Commons Attribution License, which permits use, distribution and reproduction in any medium, provided the original work is properly cited.

DOI: 10.1002/adem.202201842

J. A. Iglesias Martinez, G. Ulliac, M. Kadic
Micro Nano Sciences & Systems department (MN2S)
Institut FEMTO-ST
15B avenue des Montboucons, 25030 Besançon cedex, France

Q. Ji, C. Wang
National Key Laboratory of Science and Technology on Advanced Composites in Special Environments
Harbin Institute of Technology(HIT)
No.2 Yikuang Street, Harbin 150080, China

A. Zolfagharian
School of Engineering
Deakin University
Geelong 3216, Australia

has been made possible.^[9] In general, metamaterials can be divided into several main groups, including positive Poisson's ratio (PPR) structures such as honeycombs,^[10–12] zero Poisson's ratio (ZPR),^[13,14] buckling metamaterials,^[15,16] and negative indices mechanical metamaterials.^[17–23]

More related to our work, energy-absorbing structures are often designed using repeatable nonlinear buckling effects to achieve recoverable structures.^[24] Most traditional dampers have cylindrical shapes,^[25] and this study will also focus on cylindrical metamaterials designed by repeating the unit cells along the radial and axial directions. It is also worth noting that a metamaterial can be designed within different unit cell designs, materials, or both, so-called “graded or hybrid metamaterials”.^[26]

In parallel, the design orientation of some metamaterials comes from nature, these are so-called “bio-inspired” metamaterials.^[27,28] The graded and bioinspired metamaterials commonly exhibit superior mechanical performances compared to their regular counterparts. In this regard, Rahman et al.^[29] introduced multimaterial graded honeycomb structures with diversity in unit cell sizes. Their proposed designs disclosed better energy absorption capacity compared to a conventional honeycomb with uniform cell sizes and materials. Li et al.^[30] designed piecewise linear graded honeycombs to demonstrate high energy absorption capacity at high-crushing speeds. Hamzehei et al.^[14] designed bioinspired graded reentrant ZPR metamaterials showing simultaneous stability and high energy absorption capacity under quasi-static compression.

For everyday applications, energy absorption is crucial. This means the ability of a material or structure to absorb energy through plastic deformations, frictions, bending, and even torsion.^[31] In contrast, energy dissipation means the conversion of mechanical energy into heat through irreversible processes.^[32] The thermal dissipation channel also has a very important role to play.^[33]

In summary, here we introduce a new class of bioinspired ZPR metamaterials in cylindrical shapes in micro and macro scales for energy absorption and dissipation features. The friction-based ZPR cylindrical metamaterials do not show global buckling at high compressive strains. They also exhibit hysteresis loops under loading–unloading conditions, showing energy dissipation capability through friction. The macro cylinders also possess shape-recovery behavior^[34] after a heating–cooling process. Due to the absence of similar results in the literature, this research is highly probable to fill a gap in the industry, paving a way for industrialists to consider ZPR friction-based cylindrical metamaterials as energy absorbers/dissipators for diverse applications specifically where global buckling is undesirable.

2. Methodology Section

2.1. Microscopic Sample Fabrication

The micro-scale samples studied in this paper were fabricated by 3D direct laser writing. For this purpose, a commercial 3D printer (Photonic Professional GT+, Nanoscribe GmbH) based on the two-photon lithography method was used. The photoresist selected to produce the cylindrical metamaterials was the commercial negative tone IP-S resin showing an elastic-plastic behavior and (Nanoscribe GmbH) customized for mesoscale

applications. A drop of IP-S photoresin was deposited on an ITO-coated soda lime glass substrate and photopolymerized using a 25X microscope objective and a femtosecond laser operating at $\lambda = 780$ nm. The reference printing parameters were a laser power of 100% and a galvanometric scanning speed of 100 mm s^{-1} combined with slicing and hatching distances equal to 1 and $0.5 \mu\text{m}$, respectively. After printing, the micro-scale samples were developed for 20 min in a propylene glycol methyl ether acetate (PGMEA) solution to remove the unexposed photoresin and rinsed for 3 min in isopropyl alcohol (IPA) to clear the developer. The printed samples are cylinders with dimensions of around $[200 \times 200 \times 500] \mu\text{m}^3$. More details are provided in the Supporting Information.

2.2. Sample Testing of Microscopic Samples

To evaluate the mechanical properties of the micro samples, they were uniaxially compressed. The indenter used to induce the compression had a circular polished surface corresponding to a diameter of about 3 mm. To record the deformation process, an optical camera equipped with a lens corresponding to the 20X and 10X magnification factor was used. In order to have high-resolution pictures showing the structural details of the printed samples, the SEM microscope was used (Apreo S—Thermofisher).

2.3. Macroscopic Sample Fabrication

The macroscopic samples were made using a multijet fusion (MJF) 3D printer with Polyamide 12 (PA12). The parent material, PA-12, shows an elastic-plastic behavior. More detail can be found in the Supporting Information.

2.4. Finite Element modeling Simulations

ABAQUS explicit software package was used to perform a finite element analysis (FEA) on cylindrical metamaterials on macro and micro scales under quasi-static compression. The cylindrical metamaterials were placed between two rigid plates, as shown in **Figure 1**. The top plate moves down to compress the cylinder in a quasi-static manner. To avoid interpenetration, general contact with friction coefficients of 0.15 and 0.45 is assumed between the cells, plates, and the structure on macro and micro scales, respectively. 3D solid continuum hexahedral elements with eight nodes, so-called the C3D8R, are considered for ZPR cylindrical metamaterials. The R3D4 element type is also assumed for each rigid plate. More details regarding the FEA, including the mesh convergence study, are provided in the Supporting Information.

3. Design and Tests of Metamaterials

The ZPR cylindrical metamaterials were designed via inspiration from a parrot's beak which is composed of two jaws. When grabbing and eating the food, the bottom and top jaws play friction-based mechanisms. Friction is the mechanism a parrot used to hold and grind up or crush its food with its beak. Parrot beak is with special shape and mechanism compared with other bird beaks. It has a large relative motion between beaks wall/surfaces

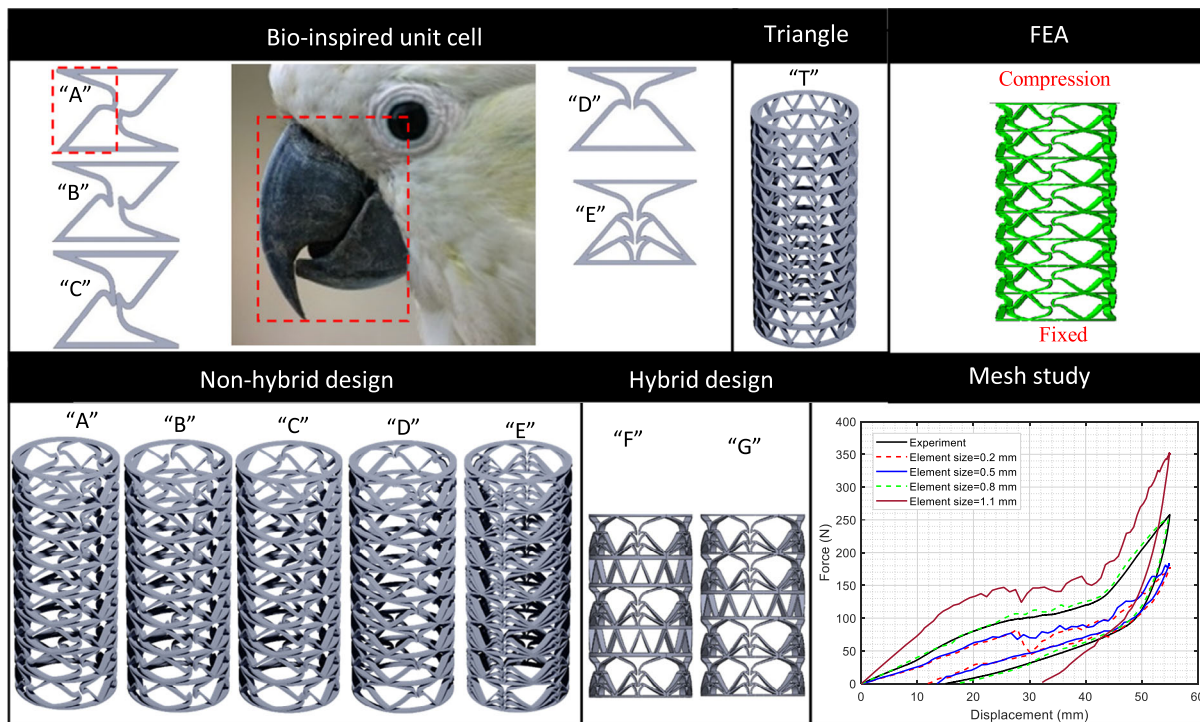


Figure 1. Design and methodologies. Five different bioinspired unit cells are designed from the inspiration of the parrot's beaks. We depict the different *meta*-cylinders constructed from primitive motifs and embedded in a periodic manner to produce cylindrical-like shapes.

introducing this friction mechanism during jaw movements. Interlock is also the mechanism assisting parrots to hold objects tightly. These are the dominant deformation modes of the proposed metamaterials in this study.

Figure 1 shows five fundamental unit cells indicated by unit cells “A,” “B,” “C,” “D,” and “E,” respectively. We considered different configurations of parrot's beaks with different curvatures for the beak at the tip. Take unit cells “B” and “C” as examples. These unit cells have sharper tips compared to the rest of the unit cells to see the effect of beak curvature on the mechanical behaviors of the metamaterials. In addition, how the layout and repetition of the parrot's beak can affect the mechanical behavior of the metamaterials, unit cells “D” and “E”. The designed unit cells and the parrot's beak are similar in both geometrical shapes and working mechanisms. The further design of cylindrical metamaterials is carried out based on hybrid and nonhybrid concepts (see Figure 1). The corresponding *meta*-cylinders are named “A,” “B,” “C,” “D,” “E,” “F,” and “G”. Detailed information on the geometrical parameters, including beam wall thicknesses and radial thickness of the cylindrical metamaterials, is provided in the Supporting Information.

The designed ZPR cylindrical metamaterials exhibit two different modes of deformation patterns, including a bi-stable (friction-based and/or interlocking) mechanism and a pure friction-based mechanism. Taking cylinder “A,” possessing bi-stable deformation patterns on this matter. Upon applying compressive displacements, the tips of the top and bottom jaws with small contact area, resulting in sliding on each other and converting the kinetic energy of the whole model to friction forces, see **Figure 2b**, which illustrates the expected mechanical behaviors

of the proposed designs through numerical simulations via finite element modelling (FEM). (Numerical model was validated by experimental results, which will be shown in a later section.) These friction-based deformation patterns lead to absorbing and dissipating energy during loadings. By continuing the mechanical loadings, the top and bottom jaws are locked into each other, so-called interlocking mechanisms, leading to maintaining the stability of the cylindrical metamaterial under quasi-static compression, see **Figure 2b** (cylinder A).

The proposed design idea with the parrot beak mechanism can realize the outstanding flexible stress–strain curve tuning by slightly changing the beak design parameter arrangement. Distinct from cylinder “A” possessing friction-based and interlocking mechanisms, cylinders “B,” “C,” “D,” and “E” exhibit different friction-based mechanisms by tuning the parrot beak design a bit. This leads to absorbing and dissipating external work through pure friction occurring in the unit cells of the cylindrical metamaterials. As seen in **Figure 2**, design B is with pure friction-based mechanism but due to the gap between beaks, the contact and friction will not happen at a small strain level leading to relatively lower stiffness and elastic modulus. The structural stiffness will then increase at contact. Design C has a large elastic modulus at initial compression with contact and sliding friction motion during compression. Design D has a relatively low elastic modulus with the same direction beak contact at a low strain level (<0.1), while the contact beaks move in the same direction during compression with no clear friction force; the elastic modulus then increases at the contact between the beak walls and the top plate. And for design E, the structural stiffness increases elastic modulus shapely, when compression strain

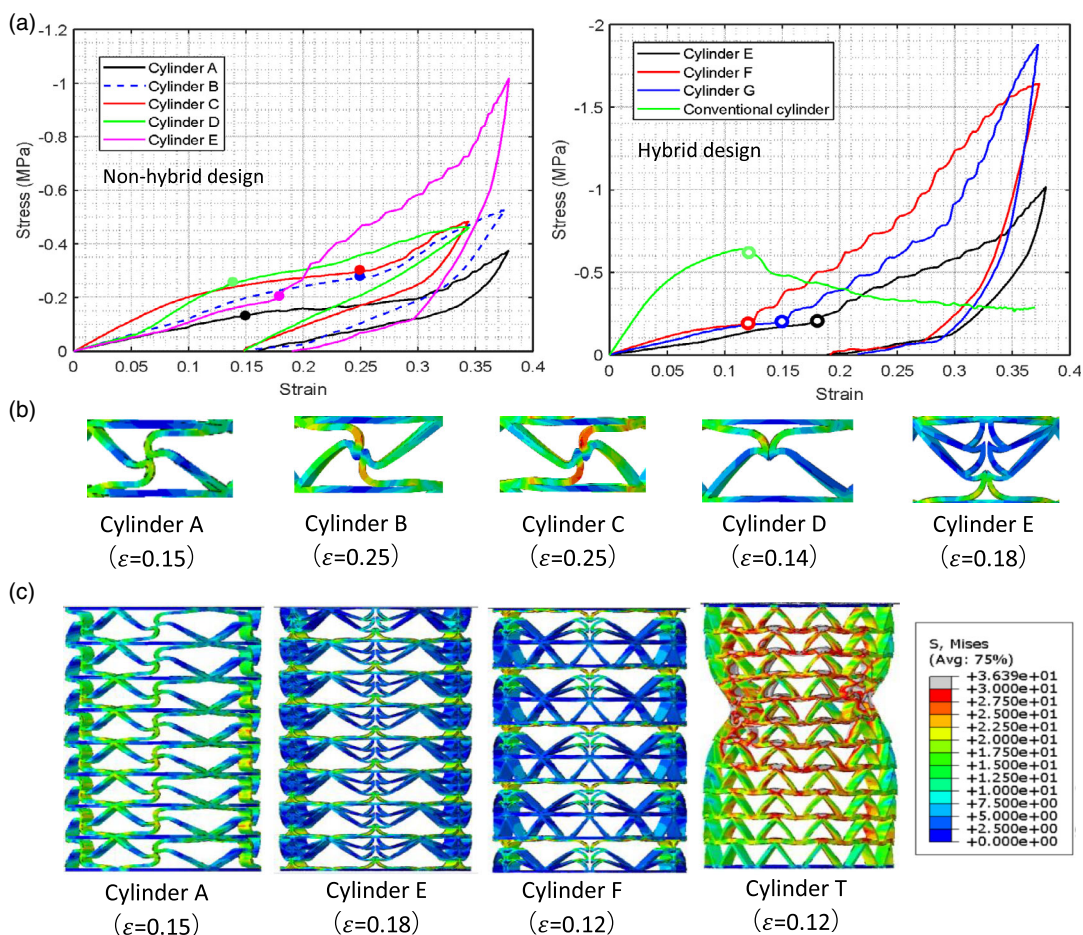


Figure 2. a) FEM Stress–strain curves for all considered macro *meta*-cylinders. b) Insets show the local deformation on some particularly interesting points of deformation. c) The color scale indicates the local von Mises stress for the deformed structure.

increases higher than 0.15, with multiple supports and contacts between beak walls.

Furthermore, hybrid designs combining the new structures and conventional triangle support layers were constructed to investigate the possibility of realizing high stiffness but keeping the unique mechanics behaviors of the parrot beak design at the same time. Designs F and G, as shown in Figure 2, are with similar stress–strain curves to designs A–E but higher stiffness and sharper stiffness increment during compression because of the high stiffness triangle support layers. Different numbers and arrangements of the triangle support layers can help to tune the stress–strain curves with a similar trend. In addition, as seen in Figure 2, thanks to the flexible and ZPR properties of the parrot beak design, the global buckling, which is usually noticed in the conventional triangle support cylinder, is successfully avoided in the hybrid designs showing their good support ability, ductility, and robustness during deformation.

3.1. Macro-scale Samples and Mechanical Behavior

The macro samples were fabricated by a MJF 3D printer from Polyamide 12 (PA 12) as seen in Figure 3a. From Figure 3b,c, one can be seen that the stress–strain curves and deformation

patterns match the numerical results and expectations illustrated in Figure 2 well. Details of the sample preparation, experimental tests, and FEM tuning and validation through the experimental tests are provided in the Supporting Information. Although the parent material used for fabrication possesses an elastic-plastic behavior, the recoverable behavior of macro cylinders after unloading can be seen in both experimental results (see Figure 3b) and the one from well-tuned FEM as shown in Figure 2. This reasonable recovery behavior is caused by the specific design of the unit cells. During loadings, the most dominant modes of deformation are friction-based. This means that the top and bottom jaws of the unit cells (left and right jaws related to unit cells “B” and “E”) experience full contact during mechanical loads. These friction-based contacts make the cylindrical metamaterials recover to their original shapes when external loading is released. It is worth mentioning that although they do not recover fully due to plastic residual strains, the cylindrical metamaterials reasonably regain their initial shapes, which will be discussed in a later section.

3.2. Micro-scale Samples and Mechanical Behavior

To investigate the scalability of our designs toward micro-structuring and thus high-resolution printed materials, the

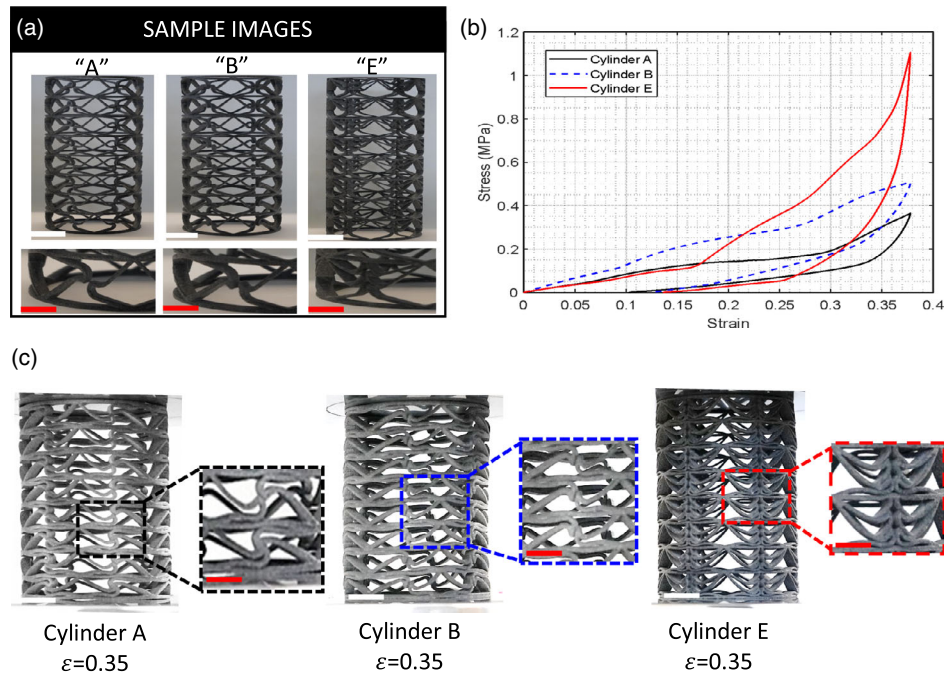


Figure 3. Macro-structures. a) Gallery of selected Optical Images of the Fabricated Macro-structures (“A,” “B,” “E”). Two scale bars are used: the white corresponds to 25 mm and the red to 10 mm. b) The corresponding measured stress–strain curves. c) Deformation patterns at strain level of 0.35.

mechanical performance of ZPR metamaterials is investigated on the micro-scale. These samples are obtained using direct laser writing with Nanoscribe GT+ (see Experimental and FEA

Section). Like the macro samples, we first depict a few examples of SEM images of the fabricated structures (see **Figure 4a**). From **Figure 4b,c**, it can be noted that similar resolutions are obtained,

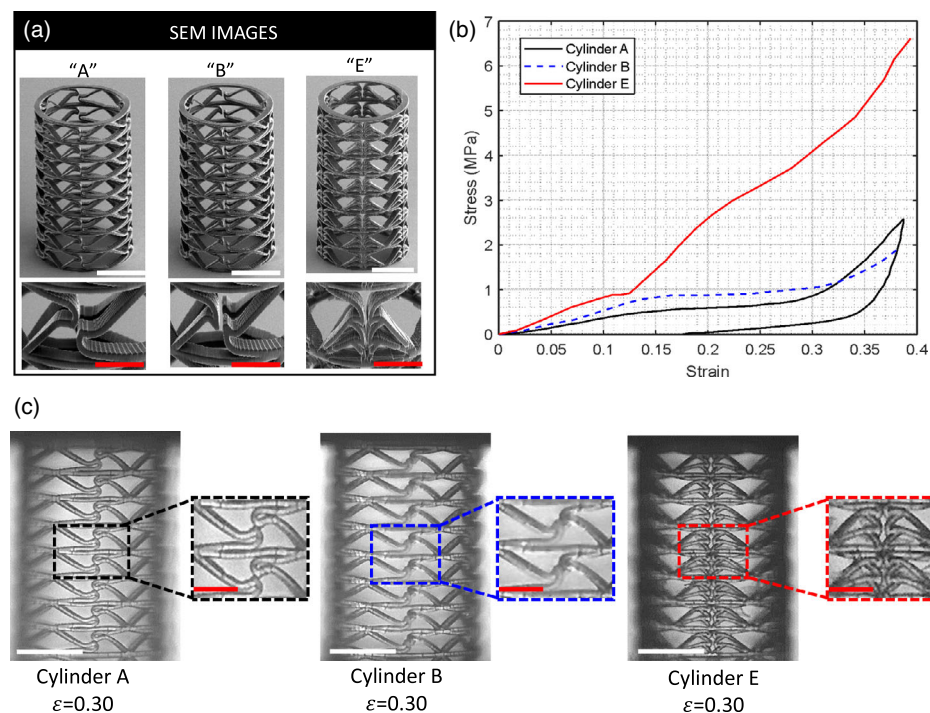


Figure 4. Micro-structures: a) SEM Images of Fabricated Micro-structures. Samples corresponding to “A,” “B,” and “E” designs are shown and a corresponding zoom onto the critical regions of the structures is depicted under each column. Two scale bars are used: the white corresponds to 100 μm and the red to 50 μm . b) The corresponding measured stress–strain curves. c) deformation patterns at a strain level of 0.3.

and the structures resemble those deformation behaviors and patterns from the previous sections (Figure 2 and 3). Movies related to micro tests are also available in the Supporting Information (Figure S11, S12 and S13).

4. Discussions

4.1. Energy Absorption and Dissipation Capabilities

We then evaluate the energy absorption and dissipation capabilities of cylindrical metamaterials on both scales using the experimentally validated FEM (a detailed validation process can be found in a Supporting Information). Firstly, nonhybrid cylindrical metamaterials, cylinders “A,” “B,” “C,” “D,” and “E,” are considered. After a loading-unloading process, the stress-strain relations of macro samples are provided in Figure 2. The friction-based deformation mechanisms lead to the appearance of hysteresis loops in force-displacement relations. This is one of the most dominant features of the metamaterials introduced in this study. From Figure 2, it is seen that at low compressive strains, until the stroke of 0.125, cylinder “C” exhibits superiority in terms of energy absorption compared to the others. This energy absorption superiority is caused by the pure friction-based mechanisms, occurring upon applying compressive loads, and the high stiffness of the parrot’s beak tips. It is worth mentioning that the only difference between cylinders “B” and “C” is the gap between the two jaws, see the related designs of unit cells “B” and “C” in Figure 1. As cylinder “C” has better energy absorption capacity compared to cylinder “B,” it can be inferred that the smaller the gap, the higher the energy absorption capacity. In addition, the only difference between unit cells “A” and “B” is different tip curvatures. The sharper tips lead to higher energy absorption capacity. This is the main reason for the higher energy absorption capacity of cylinder “B” compared to “A”. Considering the different layouts of the beak in unit cell “D” earlier hardening mechanical property can be noticed with no obvious interlock or relative motion/friction between contact pairs. But this does not guarantee higher energy absorption and dissipation capabilities compared to the friction-based mechanism. As seen in Figure 2, beyond strain 0.2, cylinder “E” possesses a dramatic increase in stress-strain relation, indicating a higher energy absorption capacity. This considerable energy absorption superiority is caused by the high stiffness of unit cell “E” due to the repetition of the jaws throughout the unit cell compared to the other unit cells, see unit cell “E” in Figure 1. In addition, reasonable recoverability, and energy dissipation capability (confined area within the stress-strain relations) can obviously be seen in all proposed ZPR cylindrical metamaterials.

For further energy absorption enhancement, we have studied hybrid designs of cylindrical metamaterials, cylinders “F” and “G”. The main reason for choosing equilateral triangles is their high stiffness compared to the other geometries. From the deformation patterns of cylinders “F” and “G” as presented in Figure 2, due to the existence of multistiffness unit cells, unit cell “E” and equilateral triangles, the cylinders “F” and “G” demonstrate both high stiffness and bi-stability properties. First, unit cells design “E” deforms under compression until full contact of the walls in unit cells, then high stiffness equilateral triangles

withstand the mechanical loads. This stage-by-stage compression of the unit cells leads to a considerable increase in energy absorption and dissipation capacity of the cylinders with reasonable stability and nonglobal buckling. It is worth mentioning that the fluctuations in stress-strain relations are induced by the friction-based deformation patterns under mechanical loads.

Following the above discussion, based on the mechanical deformation patterns, energy absorption and dissipation values from both macro and micro models were calculated. As can be seen from Figure 5a,b showing the specific energy absorption and dissipation capabilities, cylinder “E” exhibits the highest energy absorption capacity amongst nonhybrid cylindrical metamaterials on both macro and micro-scale. For hybrid cylindrical metamaterials, cylinder “F” exhibits the highest energy absorption and dissipation capabilities. It is worth mentioning that the amount of absorbed and dissipated energy comes from the FEA, and the elastic modulus is calibrated through the linear domain of the curves.

As can be seen from Figure 5c, the micro samples show higher elastic modulus compared to their macro counterparts. This is mainly caused by the material differences used for micro and macro analysis and different friction coefficients considering the surface condition variation between macro and micro sample prints. Indeed, Young’s modulus and friction coefficient of micro-samples are much higher than those printed on the macroscale. While for designs C and E, there is more obvious contact with more significant friction force generated between the contact pairs (sliding friction for design C and static friction for design E), the micro-structures with higher friction coefficient are hence with more significant higher elastic modulus for these two designs compared with other nonhybrid cylinders. Figure 5d demonstrates the higher energy absorption and dissipation capacities of micro metamaterials compared to the macro-ones. With a more obvious sliding friction phenomenon, the designs “A,” “C,” and “E” micro-structure energy dissipation SEA values are higher than macro-structure ones. The SEA values are related to both material properties and structural design.

4.2. Shape Recovery Feature

In this section, we heat the macro cylindrical metamaterials and cool them down to room temperature, to check their ability to recover to their original shapes. Nonetheless, the parrot-based cylindrical metamaterials can recover their original shapes reasonably; some plastic deformations remain in cylinders after releasing mechanical loads due to the residual plastic strains. As can be observed in Figure 5e, macro samples exhibit a fully recoverable behavior via a heating-cooling process. It means the device can be used several times when it experiences plastic deformations in severe loading, but it will disappear simply by heating. It is also worth mentioning that no fracture was seen in both micro and macro experiments during compression.

4.3. The Control of Global Buckling

This section sheds light on the capability of proposed ZPR unit cells to control the global buckling of a long cylindrical tube. In this regard, a conventional triangular cylindrical metamaterial

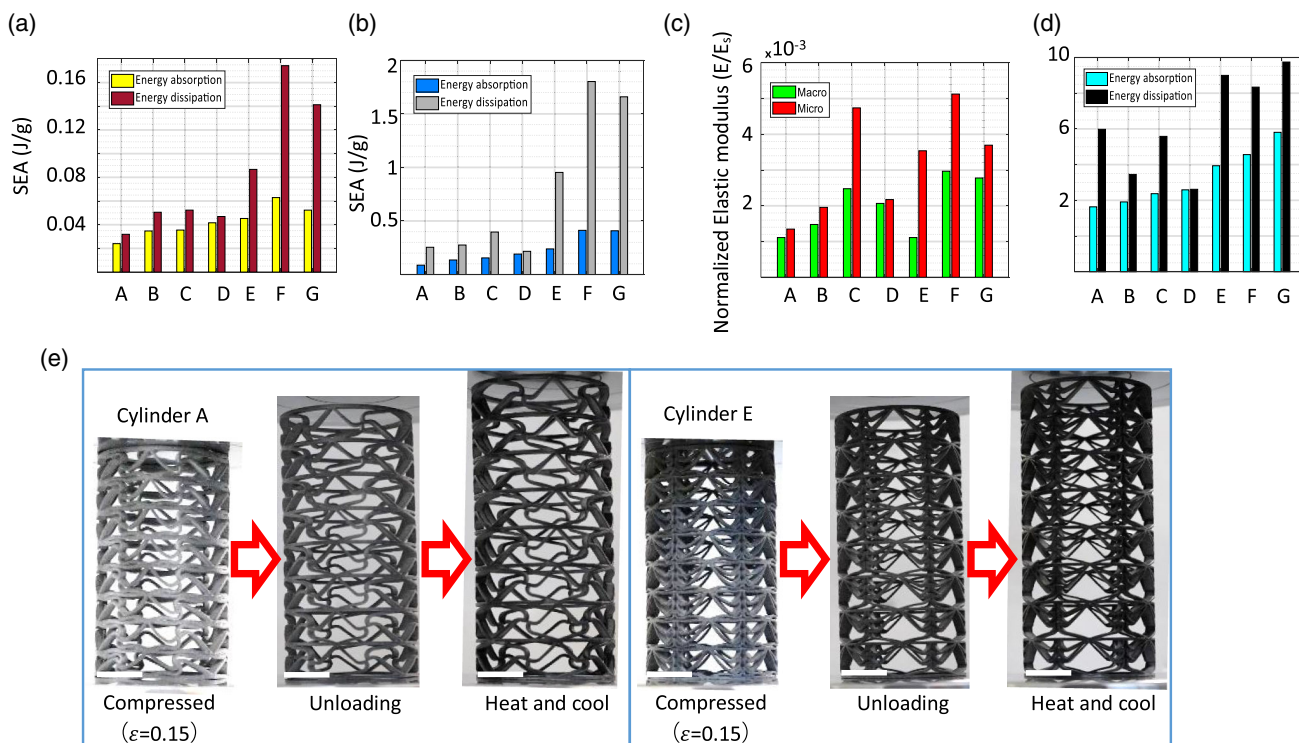


Figure 5. Energy absorption and recoverability of the *meta*-cylinders. a) Specific energy absorption and dissipation capacities for the macro and b) micro-scale structures, c) Elastic modulus for micro/macro scale samples, and d) the ratio of micro to macro scale samples in energy absorption and dissipation capacities. e) Two examples of deformed structures (compressed) are released and processed with heating–cooling treatment.

with a length-to-diameter ratio of two is considered; see the Supporting Information for more detail. As shown in Figure 2, the conventional triangular cylindrical metamaterial possesses extreme instabilities under compression. However, the simultaneous combination of proposed ZPR unit cells with triangular unit cells leads to controlling the global buckling.

5. Conclusion

In this article, we have presented a novel class of bioinspired (from parrot's beak) ZPR cylindrical metamaterials introducing the contact friction, bistability, and interlock mechanism at micro and macro scales. Different designs of the parrot beak shape lead to different combinations of these mechanisms and various desired structural mechanical behaviors, such as high support stiffness, nonglobal buckling, ZPRs, and better energy-absorbing and dissipating performance. The mechanical performance of our metamaterials has been 3D printed and investigated on both micro and macro scales. They support a high ratio of length-to-diameter compression without exhibiting global buckling. Also, the most dominating deformation patterns are friction-based and interlocking (friction and interlocking) mechanisms and exhibit superior energy absorption and dissipation capacities under a loading–unloading process. Finally, the design is seen as very robust as, although the constituent materials possess an elastic-plastic property, considerable recoverability can be seen. Furthermore, to evaluate fully recoverable behavior, the macro

cylindrical metamaterials possess shape-recovery behavior after a heating–cooling process. These results could pave the way for engineering metamaterials as energy absorbers/dissipators for diverse applications specifically when global buckling is undesirable. The rational design principles demonstrated in this work could inspire a new generation of *meta*-cylinders that cater to the demands of sustainable devices and improve their 3D-printing translation.

Supporting Information

Supporting Information is available from the Wiley Online Library or from the author.

Acknowledgements

This work was partially supported by the Natural Sciences and Engineering Research Council of Canada (NSERC), the french RENATECH network, and its FEMTO-ST technological facility. Mahdi Bodaghi and Ali Zolfagharian gratefully acknowledge the financial support and the use of the services and facilities at Nottingham Trent University and Deakin University. Thanks to Mimento and Renatech for the 3D printing at the microscale.

Conflict of Interest

The authors declare no conflict of interest.

Data Availability Statement

The data that support the findings of this study are available from the corresponding author upon reasonable request.

Keywords

3D/4D printing, bioinspired design, energy absorption and dissipation, macro and micro scales, shape recovery

Received: December 19, 2022

Revised: January 29, 2023

Published online:

- [1] J. Zhao, F. Wang, X. Zhang, L. Liang, X. Yang, Q. Li, X. Zhang, *Adv. Eng. Mater.* **2018**, *20*, 1700647.
- [2] R. Lakes, R. S. Lakes, *Viscoelastic Materials*, Cambridge University Press **2009**.
- [3] J. U. Surjadi, L. Gao, H. Du, X. Li, X. Xiong, N. X. Fang, Y. Lu, *Adv. Eng. Mater.* **2019**, *21*, 1800864.
- [4] Y. Chen, G. Hu, G. Huang, *J. Mech. Phys. Solids* **2017**, *105*, 179.
- [5] B. Florijn, C. Coulais, M. van Hecke, *Soft Matter* **2016**, *12*, 8736.
- [6] C. Coulais, E. Teomy, K. De Reus, Y. Shokef, M. Van Hecke, *Nature* **2016**, *535*, 529.
- [7] M. Brandenbourger, X. Locsin, E. Lerner, C. Coulais, *Nat. Commun.* **2019**, *10*, <https://doi.org/10.1038/s41467-019-12599-3>.
- [8] J. Hu, T. Yu, S. Yin, J. Xu, *Int. J. Mech. Sci.* **2019**, *161*, 105050.
- [9] L. M. Kalossaka, G. Sena, L. M. Barter, C. Myant, *Appl. Mater. Today* **2021**, *24*, 101088.
- [10] Y. L. Lin, Z. F. Zhang, R. Chen, Y. Li, X. J. Wen, F. Y. Lu, *Adv. Eng. Mater.* **2015**, *17*, 1434.
- [11] Z. Li, L. Shen, K. Wei, Z. Wang, *Thin-Walled Struct.* **2021**, *163*, 107759.
- [12] H. A. Rauch, H. Cui, K. P. Knight, R. J. Griffiths, J. K. Yoder, X. Zheng, Z. Y. Hang, *Addit. Manuf.* **2022**, *52*, 102692.
- [13] A. Zolfagharian, M. Bodaghi, R. Hamzehei, L. Parr, M. Fard, B. F. Rolfe, *Sustainability* **2022**, *14*, 6831.
- [14] R. Hamzehei, A. Zolfagharian, S. Dariushi, M. Bodaghi, *Smart Mater. Struct.* **2022**, *31*, 035001.
- [15] R. Hamzehei, J. Kadkhodapour, A. P. Anaraki, S. Rezaei, S. Dariushi, A. M. Rezadoust, *Int. J. Mech. Sci.* **2018**, *145*, 96.
- [16] R. Hamzehei, A. Serjouei, N. Wu, A. Zolfagharian, M. Bodaghi, *Adv. Eng. Mater.* **2022**, *24*, 2200656.
- [17] C. Qi, F. Jiang, S. Yang, A. Remennikov, *Thin-Walled Struct.* **2021**, *169*, 108314.
- [18] R. Hamzehei, S. Rezaei, J. Kadkhodapour, A. P. Anaraki, A. Mahmoudi, *Mech. Mater.* **2020**, *142*, 103291.
- [19] Z. Li, X. Li, Z. Wang, W. Zhai, *Mater. Horiz.* **2022**.
- [20] S. Rezaei, J. Kadkhodapour, R. Hamzehei, B. Taherkhani, A. P. Anaraki, S. Dariushi, *Photonics Nanostruct. Fundam. Appl.* **2021**, *43*, 100868.
- [21] H. Mansoori, R. Hamzehei, S. Dariushi, *Proc. Inst. Mech. Eng. Part L J. Mater. Des. Appl.* **2022**, *236*, 647.
- [22] A. Yousefi, S. Jolaiy, M. L. Dezaki, A. Zolfagharian, A. Serjouei, M. Bodaghi, *Adv. Eng. Mater.* **2023**, *25*, 2201189.
- [23] Z. Wang, C. Luan, G. Liao, J. Liu, X. Yao, J. Fu, *Adv. Eng. Mater.* **2020**, *22*, 2000312.
- [24] T. Frenzel, C. Findeisen, M. Kadic, P. Gumbsch, M. Wegener, *Adv. Mater.* **2016**, *28*, 5865.
- [25] K. A. Al-Saif, K. A. Aldakkan, M. A. Foda, *Int. J. Mech. Sci.* **2011**, *53.7*, 505.
- [26] H. Wang, D. Zhao, Y. Jin, M. Wang, T. Mukhopadhyay, Z. You, *Appl. Mater. Today* **2020**, *20*, 100715.
- [27] Z. Zhang, B. Song, Y. Yao, L. Zhang, X. Wang, J. Fan, Y. Shi, *Adv. Mater. Technol.* **2022**, *7*, 2200076.
- [28] W. Zhang, J. Xu, T. Yu, *Eng. Struct.* **2022**, *265*, 114490.
- [29] H. Rahman, E. Yarali, A. Zolfagharian, A. Serjouei, M. Bodaghi, *Materials* **2021**, *14*, 1366.
- [30] Z. Li, Y. Jiang, T. Wang, L. Wang, W. Zhuang, D. Liu, *Compos. Struct.* **2021**, *425*, 2019207.
- [31] R. A. Eshkoor, S. A. Oshkovr, A. Sulong, R. Zulkifli, A. K. Ariffin, C. H. Azhari, *Mater. Des.* **2013**, *47*, 248.
- [32] A. McCrary, M. S. Hashemi, A. Sheidaei, *Adv. Theory Simul.* **2022**, *5*, 2200135.
- [33] J. C. Kim, Z. Ren, A. Yuksel, E. M. Dede, P. R. Bandaru, D. Oh, J. Lee, *J. Electron. Packag.* **2021**, *143*, <https://doi.org/10.1115/1.4047414>.
- [34] X. Kuang, D. J. Roach, J. Wu, C. M. Hamel, Z. Ding, T. Wang, M. L. Dunn, H. J. Qi, *Adv. Funct. Mater.* **2019**, *29*, 1805290.